Performance of Multibeam Echosounder Backscatter-Based Classification for Monitoring Sediment Distributions Using Multitemporal Large-Scale Ocean Data Sets

Snellen, Mirjam; Gaida, Timo; Koop, Leo; Alevizos, Evangelos; Simons, Dick

Performance of multi-beam echo-sounder backscatter based classification for monitoring sediment distributions using multi-temporal large-scale ocean data sets

Snellen, M.[a,b], Gaida, T.C.[a], Koop, L.[a], Alevizos, E.[c], Simons, D.G.[a]

[a]Acoustics Group, Faculty of Aerospace Engineering, Delft University of Technology

[b]Deltares, Princetonlaan 6, 3584 CB Utrecht, The Netherlands

[c]GEOMAR Helmholtz Center for Ocean Research, 24148 Kiel, Germany

Abstract

Obtaining an overview of the spatial and temporal distribution of seabed sediments is of high interest for multiple research disciplines. Multi-beam echo-sounders allow for the mapping of seabed sediments with high area coverage. In this paper, the repeatability of acoustic classification derived from multi-beam echo-sounder backscatter is addressed. To this end, multi-beam echo-sounder backscatter data acquired on the Cleaver Bank (North Sea) during five different surveys is employed using two different classification methods, i.e., a method based on the principal component analyses and the Bayesian technique. Different vessels were used for the different surveys. The comparison of the classification results between the different surveys indicates good repeatability. This repeatability demonstrates the potential of using backscatter for long-term environmental monitoring. However, the use of different classification methods results in somewhat different classification maps. Monitoring, therefore, requires the consistent use of a single method. Furthermore, it is found that the statistical characteristics of backscatter is such that clustering algorithms are less suited to discern the number of sediment types present in the study area. The Bayesian technique accounting for backscatter statistics is therefore recommended. A strong positive correlation

27   between backscatter and median grain size for finer sediments (< 0.5 mm) using a frequency

28   of 300 kHz is observed within the study area, but an ambiguity is found for sediments with

29   median grain sizes > 0.5 mm. Consequently, for the situation considered a unique assignment

30   of sediment type to acoustic class is not possible for these coarser sediments.

31   **1. Introduction**

32   Acoustic remote sensing with multi-beam echo-sounders (MBES) is extensively used for

33   mapping the seafloor morphology because of the systems' capability to map large areas in

34   relatively short time periods. However, capabilities of these acoustic underwater techniques

35   extend beyond the determination of only the seafloor bathymetry. They also exhibit strong

36   potential for classifying the seabed sediments by investigating the sediment backscatter

37   strength that can be derived from the intensities of the received echo. The backscatter strength

38   is physically attributed to seabed properties such as sediment bulk density, seafloor roughness,

39   volume heterogeneity, discrete scatterers and sediment layering [1] [2] [3]. The contribution

40   of each factor to the backscatter strength is dependent on the complexity of the seabed,

41   acoustic frequency and angle of incidence [3]. Several regional studies have revealed a

42   relationship of backscatter to sediment properties such as median grain size [4] [5], grain size

43   distribution [6] [7] [8], or shell or gravel content [9] for a specific study area and frequency.

44   However, other studies have shown that in diverse environments additional factors such as

45   benthic fauna [10] [11], activity of benthic organisms [12], sediment compaction [13] or

46   natural hydrocarbons [14] [15] may influence the backscatter strength of the seafloor as well.

47   In general, classification methods employing measured backscatter data can be divided into

48   model-based and image-based methods [16]. Model-based methods are attributed to

49   techniques that perform inversion based on physical backscatter models either to exploit the

50   measured backscatter strength directly [17] or the angular backscatter response [18] to invert

for sediment properties (e.g. mean grain size, roughness spectrum, volume scattering coefficient). Image-based methods are based on statistical relationships and patterns within the backscatter data [19] [20]. Whereas model-based methods require accurate models for predicting the backscatter strength and well-calibrated systems for measuring backscatter strength [3] [21], image-based techniques are also applicable to relative backscatter values from poorly or uncalibrated systems.

Reference [22] gives a review of various strategies and methods employing acoustic remote sensing techniques including SBES, SSS and MBES to produce sediment or habitat maps. They present 147 studies utilizing acoustic survey techniques published during the last two decades. This is a good indicator for the intensive research already carried out and the still ongoing development in the scientific field of seafloor classification. Among others, they classify image-based methods in objective/subjective and supervised/unsupervised strategies. The classification methods applied in this study, i.e. the Principal Component Analysis (PCA) and Bayesian technique, can be referred to as image-based, objective and unsupervised strategies. The PCA and Bayesian techniques have been successfully applied to MBES backscatter in several studies [4], [20], [23], [24].

Using the full MBES acoustic data content gives the opportunity for the development of marine-landscape maps displaying topography and the seabed sediment spatial distribution simultaneously. Because of physical and biological, as well as anthropogenic processes, the seafloor is a time-varying environment. Monitoring this dynamic environment requires good repeatability of the methods for seabed sediment classification. That means the data gathering, processing, and interpretation must lead to equal results for different measurement campaigns if the environment does not change. However, regarding the use of MBES measurements for sediment classification, repeatability of the results is a topic of concern. Reference [21] points out the acoustic-instrument stability, settings, processing algorithms, range, environmental

76 conditions, and survey methods as critical factors influencing the classification results, and

77 consequently, affect repeatability. Therefore, there is a strong demand from the MBES

78 backscatter community for data quality control, standardised acquisition and processing steps

79 as well as detailed documentation of the processing chain within MBES systems [25]. In the

80 research field of seafloor classification with MBES the ultimate goal is to generate consistent

81 and repeatable results within the same area under the same settings from backscatter data

82 acquired by differing MBES systems or analysed by different processing procedures [26].

83 The goal of this paper is to apply two different classification methods to MBES backscatter

84 data acquired on different vessels during different surveys carried out in various time periods

85 and to investigate the repeatability and agreement of the resulting sediment maps. To

86 accomplish this goal, the Bayesian approach and PCA in conjunction with k-means clustering

87 approach are applied to backscatter data acquired on the Dutch vessels Zirfaea and Arca in the

88 Cleaver Bank area in the time period from 2013 to 2015. This study site consists of a

89 significant number of sediment types, and intersecting survey tracks within the source data of

90 this study allow for the investigation of the repeatability of the results. The classification

91 results are compared to ground truth data to investigate the relationship between acoustic

92 classes and sediment properties. The spatial resolution capabilities of the classification

93 methods are additionally addressed to illustrate the state of the art of methods for MBES

94 seabed sediment classification.

95 This paper is organized as follows. In Section 2 the study area and the data are described.

96 Section 3 gives an overview of the two classification methodologies that are applied. Then,

97 Section 4 presents the results from applying the classification algorithms along with

98 considerations such as the number of sediment classes that can be discerned. Section 5 is a

99 discussion of the results, addressing the repeatability of the classification, the spatial

100 resolution, the issue of assigning sediment type to the acoustic classes, as well as a discussion

101 on the ambiguity for large grain sizes. Finally, in Section 6 the conclusions are presented.

2. Study area and data

103 The Cleaver Bank area is located 160 km north-west from Den Helder in the Dutch North Sea

104 (Fig. 1) and is part of the nature protection areas in the territory of the European Union. The

105 area was formed as a terminal moraine of a glacier during the Weichselian Ice Age. The water

106 depth mainly varies between 25 m and 50 m, but is divided from north-west to south-east by a

107 70 m deep channel called the Botney cut (Fig. 1). The Cleaver Bank extends over an area of

108 about 900 km^2 and is the largest area within the Dutch North Sea with coarse sediments [27].

109 In comparison to the mostly sandy areas of the Dutch seafloor the Cleaver Bank consists of

110 the entire grain size spectrum from mud to gravel with isolated boulders. The diverse geology

111 of the Cleaver Bank seafloor is a result of the Weichselian Ice Age and is relatively well

112 preserved due to the combination of the sufficiently large depth and the rocky bottom which

113 reduces the erosive influence of waves [28].

114 The MBES data considered in this work were acquired in the Cleaver Bank area during five

115 surveys carried out within the period from November 2013 to February 2015. The entire

116 survey area is 57 km in the north-south direction and 30 km in the west-east direction. In

117 general, the survey lines are separated by approximately 1500 m except a few lines spaced

118 closer together, overlapping lines, and several cross lines (Fig. 1). The swath width ranges

119 from 90 m to 180 m depending on the water depth. Two different vessels, the Zirfaea and

120 Arca, were both equipped with a Kongsberg EM3002 single head MBES sonar system using a

121 central frequency of 300 kHz. The transmit and receive beam width are both 1.5° for nadir

122 angles. The transmitted pulse length was set to 150 μs and the number of beams were 258

123 along the entire swath. These parameters were kept constant during each survey. Furthermore,

124   the same transmitted source level, receiver gain and time-varying gain were applied during the

125   different surveys. The acquired MBES data were corrected for roll, pitch and heave.

126   Depending on the different environmental conditions, the water absorption coefficient was

127   calculated for each survey individually. The MBES data were also corrected for tidal effects.

128   To obtain a relatively good approximation of the backscatter strength from the received

129   acoustic echo several steps are carried out within the Kongsberg MBES. The system corrects

130   in real time for transmission loss (attenuation and geometrical spreading), insonified area as

131   well as for transmission and reception beam pattern [29]. However, the real-time correction

132   for the insonified area assumes a flat seafloor. Therefore, the backscatter data is corrected for

133   the seafloor bathymetry slope in post processing to obtain the true insonified area [30].

134   However, some of the real-time correction performed by Kongsberg still includes

135   simplification of the marine environment (e.g. constant absorption coefficient, flat seafloor

136   assumption for reception process) which might affect the true backscatter strength [26]. In

137   addition, a MBES calibration that would account for the alteration of sonar transducers'

138   sensitivities or deviation of the system configuration from the manufacturer specification was

139   not performed. Taking these factors into account, strictly speaking, the employed acoustic

140   data represent a relative rather than absolute backscatter strength because the data might still

141   not be entirely independent of the MBES configuration or environmental impacts. Therefore,

142   we are using the term backscatter data or backscatter values in this paper instead of

143   backscatter strength.

144   For validation and assignment of sediment type to acoustic class, 104 Hamon and Van Veen

145   grab samples were taken during four different surveys in 2000, 2013, 2014 and 2015 (Fig. 1).

146   The grab samples were sieved to separate the gravel and shell fragments from the sand and

147   mud fraction. The latter part was analysed by laser-diffraction granulometry. The percentage

148   of the different grains was used to classify the grab samples after the Folk scheme [30].

149   Almost no shell fragments or other biological particles were found to be present in the grab

150   samples. Because the seafloor dynamics of the Cleaver bank are low, the grab samples from

151   2000 are considered to be valid.

152
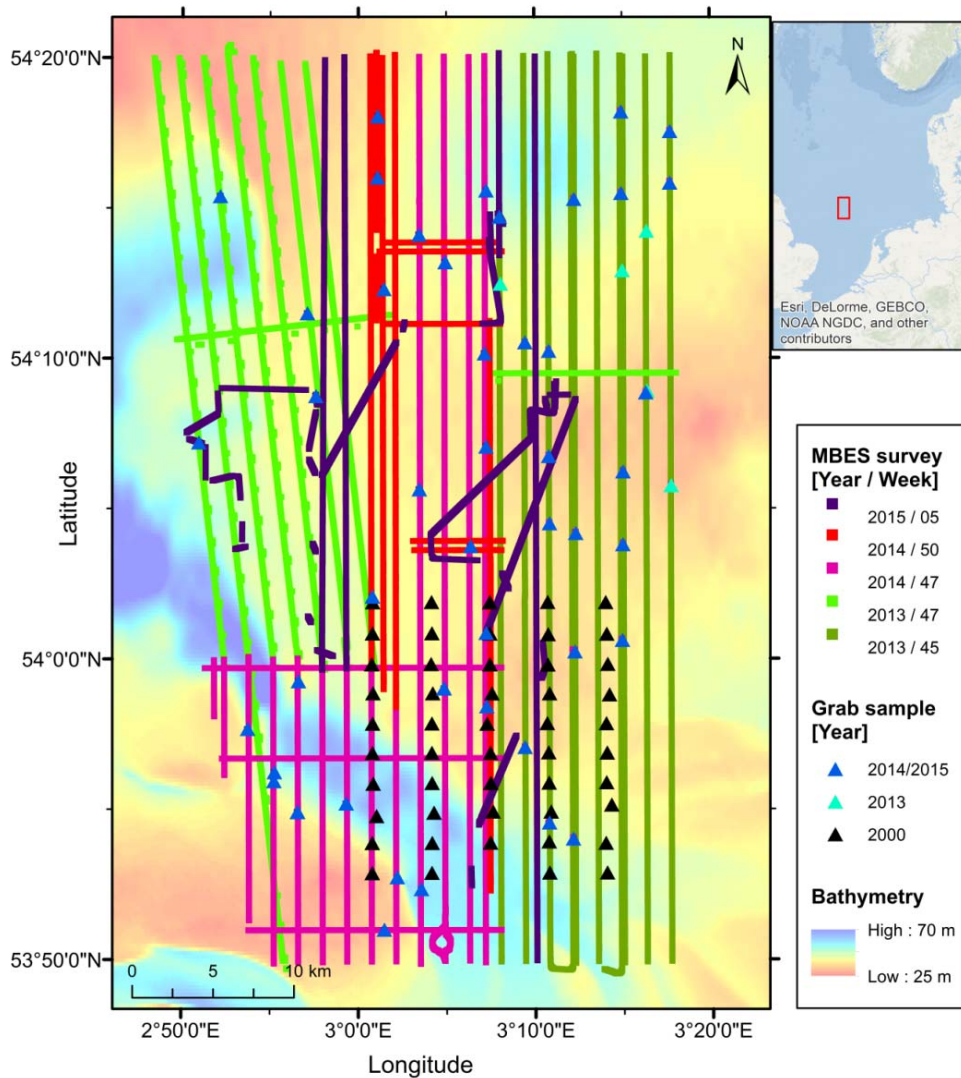
Fig. 1 . MBES tracks of five different surveys carried out from 2013 to 2015 are plotted over the bathymetry of the Cleaver Bank. Bathymetry is received from EMODnet [31]. Grab samples taken in the years 2000 and 2013 to 2015 are denoted by triangles.

3. Classification methods

157   In this study two unsupervised sediment classification methods, the Bayesian technique and

158   PCA in conjunction with k-means clustering, are applied to the MBES data of the Cleaver

159　Bank. The Bayesian technique for seafloor classification was developed in [23] where also a

160　detailed theory description is given. It has since been used in [4], [20], [24], and [32]　among

161　others. This section provides a brief overview of the basic concepts and the relevant

162　processing steps to generate the sediment maps of the Cleaver Bank. The theory of PCA was

163　first introduced by [33] [34]. Today many different variations of PCA exist which are adapted

164　depending on the application purposes. A very detailed explanation of the application to

165　MBES data is given by [20].

166　**3.1　Bayesian technique**

167　Assuming that a beam footprint contains a large number of scatter pixels, based on the central

168　limit theorem, the backscatter strength per beam footprint can be assumed to be Gaussian

169　distributed [23]. A scatter pixel here is the instantaneously insonified area of the sea floor

170　within a beam footprint of the MBES. Given a constant frequency and angle of incidence, the

171　backscatter strength is dependent on the seabed properties. It follows that if a survey area has

172　a total of m different sediment types, with specific seabed properties, then the backscatter

173　histogram from a selected oblique beam of the echo-sounder should be represented by a

174　combination of m Gaussian distributions. Consequently, the model for the histogram of

175　measured backscatter values per beam can be written as

$$f(y_j|\mathbf{x}) = \sum_{k=1}^{m} c_k \exp\left(-\frac{(y_j - \bar{y}_k)^2}{2\sigma_{y_k}^2}\right) \tag{1}$$

176　where $f(y_j|\mathbf{x})$ is the value of the model at backscatter value y_j, and $\mathbf{x}$ is the vector

177　containing the unknown parameters, $\mathbf{x} = (\bar{y}_1, ..., \bar{y}_m, \sigma_{y_1}, ... \sigma_{y_m}, c_1, ..., c_m)$, i.e. the means

178　$\bar{y}_k$, standard deviations σ_{y_k} and coefficients c_k of the Gaussian distributions that represent

179   each seafloor type. By fitting the above model to the measured histogram all unknowns are

180   determined.

181   With a new data set, one may not know how many sediment types there are in the survey area.

182   By conducting a χ^2 goodness of fit test, the optimal number of Gaussians m can be

183   determined where χ^2 is defined as:

$$\chi^2 = \sum_{j=1}^{M} \frac{\left(n_j - f(y_j|\mathbf{x})\right)^2}{\sigma_j^2} \tag{2}$$

184

185   Here the n_j denote the number of measurements per bin (in our case the bin size is 0.5 dB) of

186   the previously mentioned histogram and M is the total number of bins in the histogram. For

187   the n_j a Poisson-distribution is postulated[1]. The variances σ_j^2 are thus equal to n_j. The

188   goodness of fit statistic is χ^2 distributed with $v = M - 3m$ degrees of freedom. The goodness-

189   of-fit criterion is then further defined as the reduced-χ^2 statistic ($\chi_v^2 = \chi^2/v$) having a value

190   close to one [35, pp. 68, 195 - 197]. The value of m for which a further increase of m does not

191   generate a better fit of the model to the histogram, as quantified by the reduced-χ^2 measure, is

192   taken to be the number of seafloor types that can be discriminated in the survey area based on

193   the backscatter data.

194   For the classification, the Bayes decision rule is applied, where there are m states or

195   hypotheses. These hypotheses correspond to the m seafloor types present in the surveyed area.

196   From Bayes and assuming all hypothesis to be equally likely, it is found that the intersections

---

[1] The requirements for an event being Poisson distributed are that (1.) E is the number of times the event in question occurs in an interval of time or space. (2.) $E \in 0 \cup \mathbb{N}$ (3.) The events are independent. (4.) The probability of the event occurring does not vary with time. (5.) Two events cannot occur at the same time. (6.) The probability of an event in a small interval is proportional to the length of the interval.

197   of the *m* Gaussian PDFs provide the *m* non-overlapping backscatter acceptance regions,

198   corresponding to the *m* seafloor types.

199   3.2   Principal component analysis and k-means clustering

200   PCA is a statistical method to reduce the complexity of a dataset while preserving most of the

201   information content. This is achieved by transforming the original data set consisting of *p*

202   (potentially) correlated variables to a new data set of $\ell = 1, 2,\ldots, p$ uncorrelated variables Y_ℓ,

203   the so-called principal components (PCs). Each PC can be seen to account for a part of the

204   variation in the feature values of the original data set. Therefore, the size of the original data

205   set can be reduced by considering only the PCs representing a significant portion of the data

206   variability.

207   The *n* measurements of the *p* variables, often called features, are summarized in an $(n \times p)$

208   data matrix. To account for different magnitudes of the features, the data are standardized,

209   where for each feature the mean is determined and subtracted from the measurements of that

210   feature. In addition, the features are divided by their standard deviation. The matrix **F** contains

211   these standardized measurements. The first step of PCA is the calculation of the covariance

212   matrix of **F** as

$$\mathbf{R} = \frac{1}{n} \sum_{j=1}^{n} \mathbf{F}_j^{T} \mathbf{F}_j \tag{3}$$

213   with $\mathbf{F}_j$ the jth row of the matrix **F.** Superscript T denotes the transpose. The second step is to

214   determine the eigenvectors and the corresponding eigenvalues of **R** by solving

$$\mathbf{RA} = \mathbf{A\Lambda} \tag{4}$$

215   with $\mathbf{A}$ the (p x p) eigenvector matrix whose columns are the eigenvectors $\boldsymbol{a}_\ell$ and $\boldsymbol{\Lambda}$ the (p x

216   p) eigenvalue matrix where the diagonal elements are the corresponding eigenvalues λ_ℓ of the

217   covariance matrix $\mathbf{R}$.

218   The obtained eigenvector matrix $\mathbf{A}$ is used to transform the original data set $\mathbf{F}$ into the new

219   data set consisting of the PCs. Thus, the original measurements $\mathbf{F}_j$ can be written as a sum

220   over the eigenvectors, i.e.,

$$\mathbf{F}_j = \mathbf{Y}_j \mathbf{A}^\mathrm{T}$$

(5)

221   with the coefficients for the eigenvectors contained in the row vector $\mathbf{Y}_j$ of matrix $\mathbf{Y}$. Thus,

222   one finds

$$\mathbf{Y}_j = \mathbf{F}_j (\mathbf{A}^\mathrm{T})^{-1}$$

(6)

223   where the full matrix $\mathbf{Y}$ is of size (n x p), as is the original matrix $\mathbf{F}$, and contains for the n

224   measurements the p coefficients for the eigenvectors. In general, although different definitions

225   exist, the ℓth column $\boldsymbol{Y}_\ell$ of $\mathbf{Y}$ is considered as the ℓth PC, given by

$$\mathbf{Y}_\ell = \mathbf{F} \boldsymbol{a}_\ell$$

(7)

226   The amount of variability in the original data set which is accounted for by the PC $\mathbf{Y}_\ell$ is

227   quantified by the eigenvalue λ_ℓ. Based on these eigenvalues a subset of PCs can be selected

228   that represent the majority of the variations in the measurements. For this work, the subset

229   was selected such that 70% to 90 % of the data variability is accounted for. These PCs are

230   then supplied to the k-means algorithm to group the PCs into different clusters [36].

231 The k-means clustering algorithm aims to assign the n data points for each of the PCs into k

232 predefined clusters S_i $(i = 1,…,k)$. Thereby the sum of the squared Euclidean distance

233 between the data points and the average of all data points within the cluster, i.e., the so-called

234 cluster centroid, is minimised. The minimisation problem is thus

$$min \sum_{i=1}^{k} \sum_{x_s \epsilon S_i} |x_s - c_i|^2 \tag{8}$$

235 where x_s is a data point within the cluster i and c_i is the cluster centroid of the cluster i.

236 The application of the k-means algorithm to a dataset requires a predefined number of clusters

237 k. However, the estimation of how many clusters to use is a well-known issue in unsupervised

238 classification methods [37] and is in general the most subjective part of a cluster analysis. In

239 this study three different statistical methods are applied to the MBES backscatter dataset to

240 determine the number of clusters.

241 The statistical methods are applied to the output of the clustering techniques using varying

242 numbers of clusters. The first method, the gap statistic, was proposed by [38]. This method

243 calculates the overall within-cluster variance of the dataset and compares this value to an

244 expected value calculated for an appropriate reference distribution. The estimated number of

245 clusters is defined where the logarithmic overall within-cluster variance value is minimized. A

246 detailed mathematical description is found in [38]. The second method, the Silhouette

247 statistic, is developed by [39]. The average distance of the observations within the clusters and

248 the average distance of the observations to the data points in the nearest clusters is calculated

249 for each number of clusters. The values are called the Silhouette coefficients. The optimal

250 number of clusters is selected where the Silhouette coefficient is maximized. Finally, the

251 David-Bouldin criterion is also used in this study [40]. This method examines the ratio of the

252   within-cluster distance and between-cluster distance. The optimal clustering solution is

253   represented via the smallest David-Bouldin index. In [38], the performance of several cluster

254   number estimation methods including the gap statistic and the Silhouette coefficient was

255   investigated. That study demonstrated that the gap-statistic performs most efficiently.
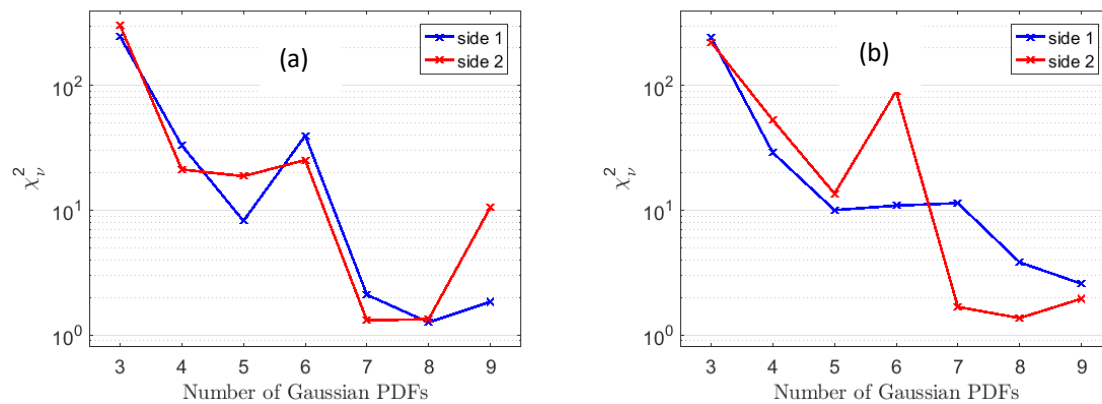
4. Results

257   In this section, the results of the two classification methods are presented. Both methods

258   employ the MBES backscatter data for the classification of the seafloor.

4.1   Bayesian method

260   For the application of the Bayesian method we use receiving beams between 20° and 60°. The

261   beams between nadir and 20° are not used because firstly, there are too few scatter pixels to

262   meet the central limit theorem requirement and secondly, these beams are less sensitive to

263   sediment properties (e.g. roughness) variation than the outer beams [41]. Often receive beams

264   beyond 60° can also be used for classification but for the data considered here, those beams

265   tended to be too noisy to yield reasonable results.

266   The estimation of the optimal number of classes is a well-known issue in unsupervised

267   classification methods [37]. For the Bayes method, however, a statistically sound approach is

268   available. Here, the curve fitting procedure as described in Section 3.1 is executed for

269   increasing numbers of sediment types m. The number of sediment types present in the area is

270   taken as that value of m for which a further increase in m does not result in a further

271   improvement of the fit. The goodness of fit is quantified through the reduced χ_v^2 statistic. For

272   the Cleaver Bank data, it is found that a maximum of seven sediment types can be

273   discriminated based on the available backscatter data. Fig. 2 shows an example of the χ_v^2

274   statistic for an increasing number of Gaussians and for the 48° beam from nadir, for both the

275   2013 and 2014/2015 data, as well as the two sides (starboard and port). It is seen that for the

276   2013 data as well as for side 2 of the 2014 and 2015 data the use of 7 Gaussians provides a

277   very good fit between modelled and measured histogram, with the χ_ν^2 statistic being close to

278   1. An example, indicating that sometimes the χ_ν^2 statistic is inconclusive about the number of

279   Gaussians, is shown for side 1 in Fig. 2b. In general, such behaviour is found for a limited

280   number of cases and, therefore, these results are discarded when determining the number of

281   sediment types. These analyses have been carried out for beam angles between 46° and 60°

282   and for all surveys, not all of which are plotted here. In general, a single outer beam is used to

283   determine the number of Gaussians, but given that our data is noisy, we choose to investigate

284   a number of beams. The use of 7 Gaussians is found to reproduce the measurements best.


285

286   **Fig. 2. The reduced χ_ν^2 statistic for the 48° beam angle. The two curves are for the two sides of the echo-sounder**
287   **respectively. a) 2013 data and b) 2014 and 2015 data.**

288   As an example, Fig. 3 presents the result of the fitting procedure for seven Gaussians. Here

289   the histogram of the measured backscatter data n_j (black line with error bars) per 0.5 dB bin is

290   almost hidden by the modelled backscatter in red. The variance of the measured data is

291   indicated by the error bars. Also seen are the 7 Gaussians used for the curve fitting in black.

292   After a good fit is found per beam angle and per experiment, the intersections of the unscaled

293   Gaussians are used to derive the ranges of backscatter, corresponding to the different acoustic

294   classes, from which the acoustic class map is derived as explained in [23]. Acoustic classes 1-

295   7 correspond to the Gaussians from left to right, and from lowest to highest backscatter

296   values.
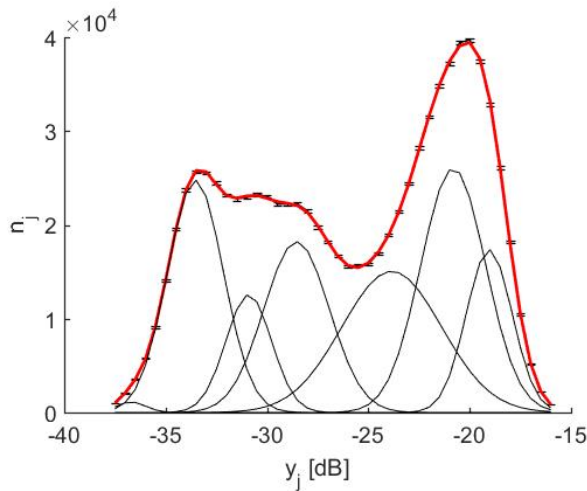
Fig. 3. Shown here is the histogram of the measured backscatter data n_j per 0.5 dB bin y_j from the data collected in 2014 and 2015 (black line with error bars) which is almost hidden by the modelled $f(y_j|x)$ in red. Also displayed are the 7 Gaussians in black.

302   The resulting classification map is shown in Fig. 4 where each acoustic class is presented with

303   a separate colour. Colours have been selected such that from green to purple the backscatter

304   value increases.

4.2   PCA and k-means clustering

306   PCA in conjunction with a clustering algorithm is a common unsupervised classification

307   technique for seafloor classification based on backscatter [24], [19]. This technique is

308   applicable to relative backscatter values and, therefore, does not necessarily require calibrated

309   MBES. In recent studies, this method was also applied to backscatter and bathymetry

310   simultaneously [20], [4]. However, in this study PCA and k-means clustering are only applied

311   to backscatter so that a direct comparison with the classification from the Bayes method can

312   be made.

313   As with the Bayesian technique, for PCA and k-means clustering, beam angles from 20° to

314   60° are considered. The backscatter data are averaged over seven pings in the along-track

315   direction and over an angle range of 2° to 4° in across-track direction. To eliminate the

316   angular dependency of backscatter the global Z-score approach is applied, which is the

317   subtraction of the mean value from the backscatter value, and then divided by the standard

318   deviation at each angle [20] [42] (henceforth simply referred to as backscatter). To obtain the

319   same resolution among the entire survey area, surface patches of 10 m x 10 m are constructed

320   similar to [32].

321   For each surface patch eight statistical features of the backscatter distribution are calculated

322   (Table 1). The arithmetic mean gives the averaged backscatter value within the patch. If the

323   distribution is not symmetric, the median value differs from the mean and provides the middle

324   of the distribution. Therefore, the median can be considered as an additional valuable feature.

325   The mode represents the value with the highest occurrence within a patch and defines the

326   main tendency of the feature [20]. The standard deviation shows the variability of the

327   backscatter and might be valuable to characterise the heterogeneity of the sediment. Due to

328   the fact that outliers are removed during processing, the minimum and maximum value can be

329   used to define data extremes and might also indicate specific characteristics of the seabed. The

330   higher statistical moments, skewness and kurtosis, are measures of the shape of a probability

331   distribution. In previous studies it was shown that the K-distribution can be used to describe

332   the skewed distribution of backscatter data for all sediment types and the shape parameter of

333   the K-distribution can be used as tool for seafloor classification [43] [44] [32] [45]. Therefore,

334   the skewness and kurtosis might provide valuable information about the sediment distribution.

335   To identify the most valuable of these features, PCA is applied. PCA analysis indicates that

336   the first 3 PCs contain most of the data variability of around 85%. Fig. 5 displays the ratio of

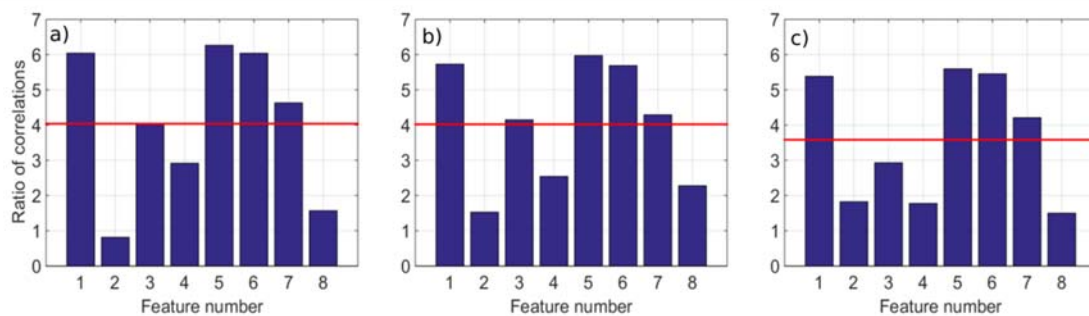337   the sum of the correlation between the first three PCs and the eight backscatter features to the

16

338
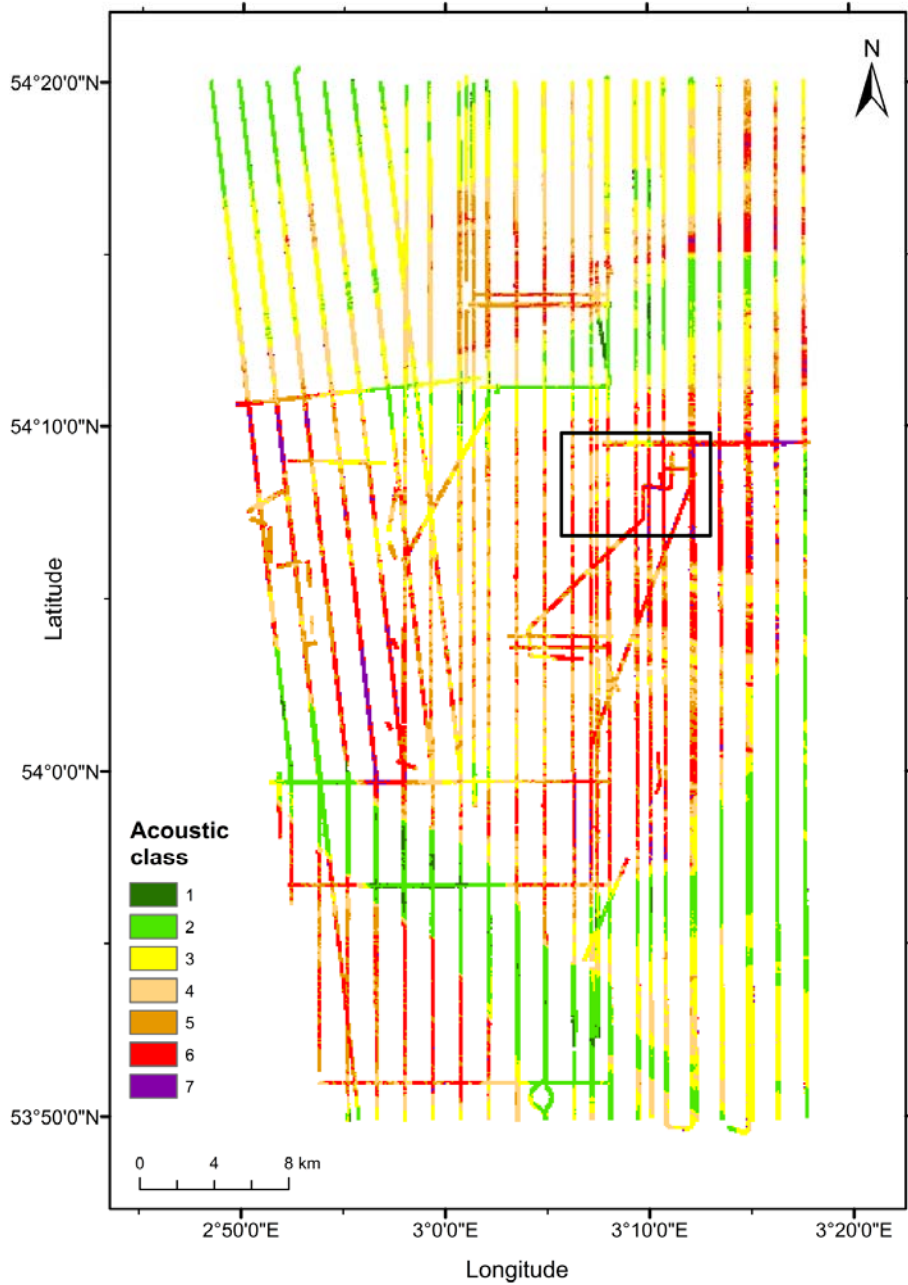
Fig. 4. Acoustic classification result of the Bayesian technique. The grid is resampled to a size of 100 m by 100 m using the mode value of the finer grid. The black square indicates the extent of the area zoomed in Fig. 10.

sum of correlation between the remaining PCs and the eight backscatter features. In reference [20], the threshold value has been chosen considering three conditions: (1) it is similar to the mean value (red line), (2) it includes an adequate number of features for PCA and (3) it

344   generates consistent results for each survey. Considering these three conditions the mean,

345   median, mode and the minimum of the backscatter data are revealed as the most informative

346   features. PCA analysis indicates that the first 3 PCs contain most of the data variability of

347   around 85%. Fig. 5 displays the ratio of the sum of the correlation between the first three PCs

348   and the eight backscatter features to the sum of correlation between the remaining PCs and the

349   eight backscatter features. In [20], the threshold value has been chosen considering three

350   conditions: (1) it is similar to the mean value (red line), (2) it includes an adequate number of

351   features for PCA and (3) it generates consistent results for each survey. Considering these

352   three conditions the mean, median, mode and the minimum of the backscatter data are

353   revealed as the most informative features.

354   **Table 1. Backscatter features considered in the first application of PCA.**

| Number	1	2	3	4	5	6	7	8
BS feature	Mean	Std. deviation	Skewness	Kurtosis	Median	Mode	Min.	Max.

355

356   **Fig. 5. Ratio of the sum of the correlation between the first 3 PCs and backscatter features to the sum of the**
357   **correlation between the remaining PCs and backscatter features. The different surveys are considered separately: a)**
358   **2013, b) 2014 and c) 2015. The red line indicates the mean value of the ratio of correlation.**

359   These features were used as an input for a second application of PCA to further reduce the

360   complexity of the dataset and simplify the application of the k-means clustering. The analysis

361   shows that the first PC accounts for 98% of the data variability which indicates high

362   correlation between the selected four backscatter features. Therefore, only this component is

363   used in the k-means clustering.

364   To estimate the optimal number of acoustic classes that can be distinguished within the data,

365   the gap statistic, silhouette coefficient and Davies-Bouldin method are applied. The methods

366   use the output of the k-means algorithm which is applied to varying numbers of clusters in the

367   range from 2 to 10. The results of each method are plotted in Fig. 6. Each method has

368   different magnitudes of criterion values and therefore the values are normalised. The optimal

369   number of classes estimated and suggested by each method is two, which is indicated by the

370   red dots. This can be understood from Fig. 3, showing a histogram of the backscatter data.

371   Clearly two main peaks are present. These two main peaks are estimated as individual clusters

372   by the statistical methods. However, this is in disagreement with both the ground truth data

373   which reveals eight sediment types, and the Bayesian technique which estimates seven

374   clusters, similar to the ground truth data.

375
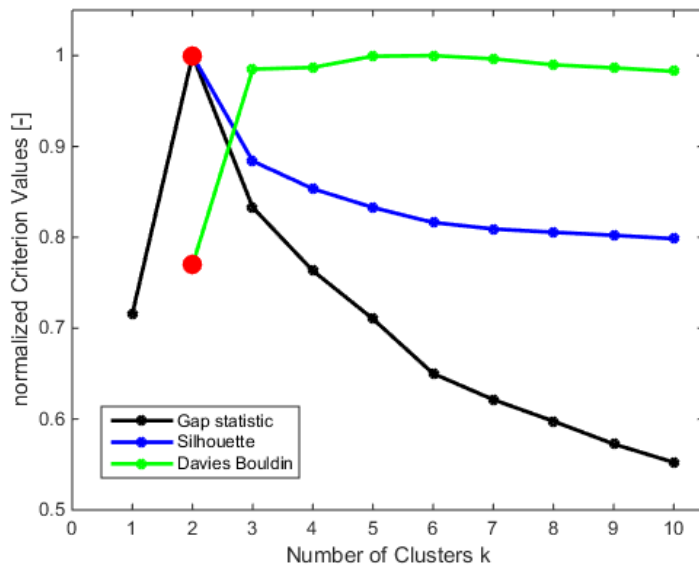
Fig. 6. Estimating the number of clusters via Gap statistics, Silhouette coefficient and Davies-Bouldin method. Red circle indicates optimal number of clusters estimated by each method.

376
377

378   To further investigate why the statistical methods only identify two clusters within the

379   backscatter data the Gap statistics, Silhouette coefficient and Davies-Bouldin methods are

380   applied to synthetic backscatter histograms. Four different synthetic backscatter histograms

381   with varying degree of overlap and number of main peaks are shown in Fig. 7. Fig. 7c

382 represents a similar backscatter histogram as the measured histogram (Fig. 3). Again, the

383 methods only identify the two main peaks as individual clusters. Modelling backscatter

384 histograms with four and seven main peaks, respectively (Fig. 7b and Fig. 7d) and applying

385 the statistical methods show that even when the individual peaks are clearly visible, the

386 overlap hampers the clustering methods' ability to identify the peaks as individual clusters.

387 Only the synthetic backscatter histogram in Fig. 7a having peaks with very distinct

388 separations were correctly found to have four clusters by the three methods. This

389 demonstrates that the statistical methods trying to estimate the number of clusters require a

390 clear segmentation of the individual clusters which is not always the case for backscatter data.

391 Seafloor backscattering is a random process having statistical fluctuation leading to a natural

392 overlap of the backscatter data [1]. In addition, the mostly heterogeneous seabed does not

393 show clear boundaries between sediment types, increasing the overlap within the measured

394 backscatter data. In this study, the backscatter features are highly correlated. It is hypothesized

395 that for situations where this correlation is less, or when additional information such as those

396 derived from bathymetry are added, the overlap in clusters diminishes and separation between

397 clusters would be higher. The Bayesian technique accounts for the statistical fluctuation of the

398 backscatter data [23] and, therefore, is able to distinguish between individual overlapping

399 clusters in this study as well. This method estimates seven clusters to be present in the data

400 set. Based on the result of the Bayesian technique and taking into account the fact that the

401 ground truth data reveals eight sediment types (defined by the Folk scheme) (Section 4.3) as

402 well as to have consistency between the Bayes and PCA/k-means methods, k-means

403 clustering is applied with a choice of seven clusters.
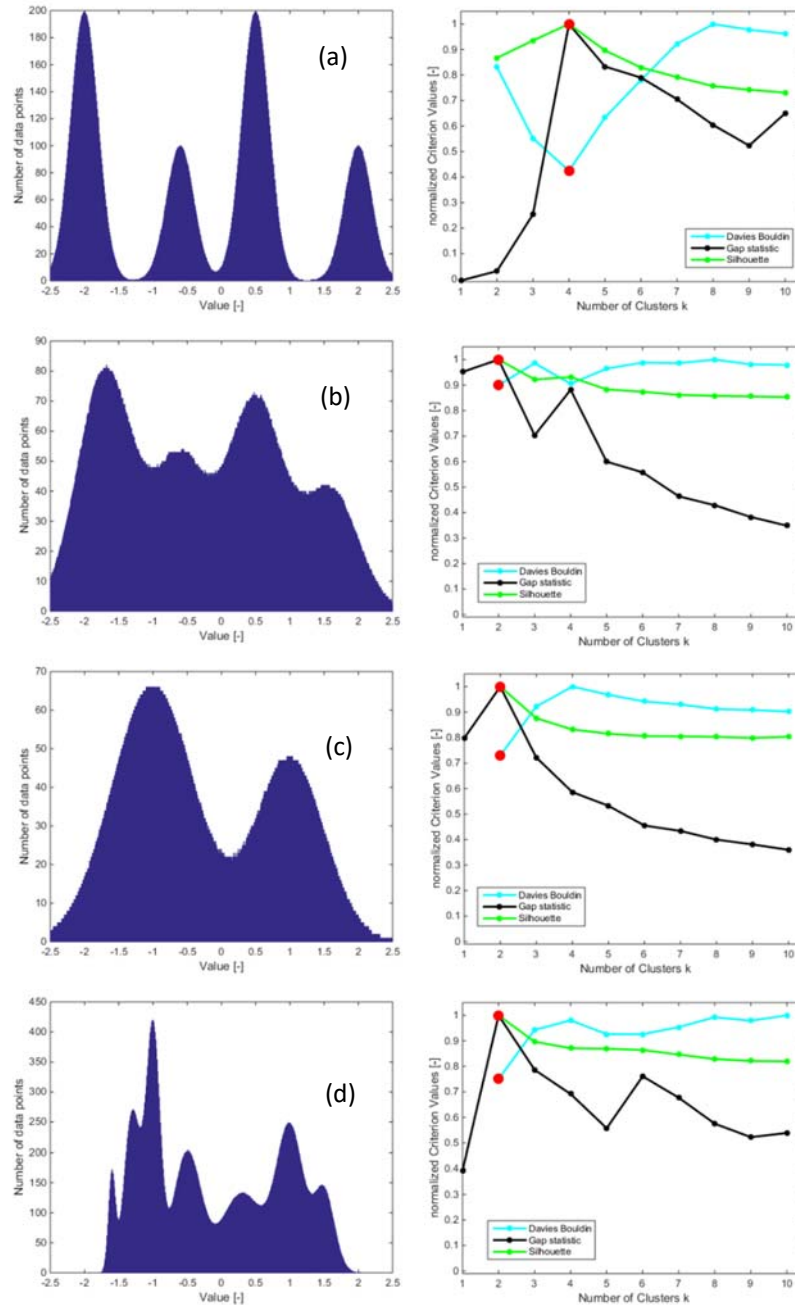
Fig. 7 Synthetic histograms generated by modelling a different number of Gaussians (left). Application of Davies Bouldin, Gap statistic and Silhouette coefficient to synthetic data (right). (a) 4 clearly segmented Gaussians. Each statistical method gives 4 clusters as a result. (b) 4 Gaussians with overlapping segmentation. Statistical methods are not able to identify 4 individual clusters. (c) 2 Gaussians representing a hypothetical histogram of backscatter data of the Cleaver Bank. Statistical methods identify 2 clusters. (d) 7 Gaussians that approximately reproduce the histogram of the backscatter data of the Cleaver Bank but with added separation. Even in this modelled and simplified case, statistical methods suggest 2 clusters as the optimal number.

Acoustic classes are obtained from the output of the k-mean clustering by sorting the seven

clusters according to the averaged backscatter value of each cluster. Fig. 8 displays the

414 resulting acoustic classification map. Compared to the acoustic map of the Bayesian approach

415 (Fig. 4) acoustic class 1 and 7 have a very large contribution to the entire map. The resulting

416 map can be divided in seven distinct areas based on the criterion of high and low acoustic

417 classes as well as homogeneity and heterogeneity. The most of obvious areas are 1) the

418 heterogeneous centrum consisting of mainly acoustic classes with higher backscatter values;

419 2) and 3) the homogenous north-western and south-eastern parts with lower backscatter

420 values; 4) the very homogeneous Botney cut characterised by only acoustic class number 1 in

421 the south of the central part; 5) the south-western area which is characterised by

422 homogeneously distributed sediments with high backscatter values; and 6) just north of the

423 centre a stripe of low backscatter, homogeneously distributed sediment is located; 7) further

424 north in the north-eastern part of the map a very small stripe of heterogeneous, high acoustic

425 classes, sediment is present. These distinct areas are also visible in the acoustic map of the

426 Bayesian technique (Fig. 4). The main differences to consider belong to a shift between the

427 acoustic classes, in particular at the low and high classes. A more detailed view and

428 discussion of these maps follows in sections 5.1 and 5.3.

429 **4.3   Ground truth**

430 The analyses of the grab samples indicate the presence of eight different sediment Folk

431 classes, ranging from sandy mud to sandy gravel in the Cleaver Bank. The grab samples

432 containing gravel are located in the northern and middle part of the survey area as well as in

433 the south of the Botney cut (see Fig. 13). Sandy mud grab samples are only available within in

434 the Botney cut and muddy sand occurs mainly around the Botney cut. The grab samples from

435 2013 to 2015 are located directly on the MBES track whereas some grab samples taken in

436 2000 are located about 500 m away from a MBES survey line (Fig. 1).
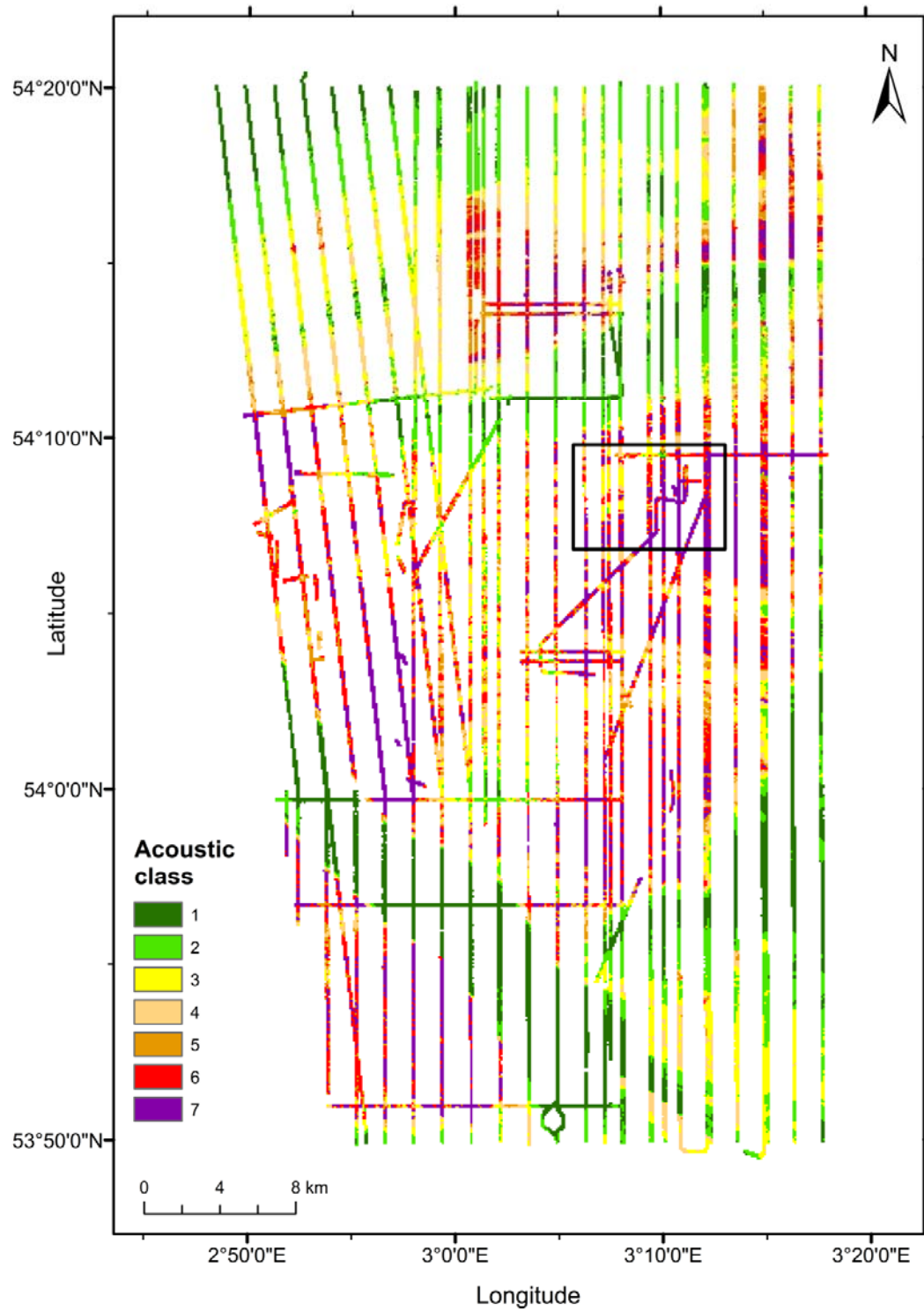
438   **Fig. 8. Acoustic classification result of PCA in conjunction with k-mean clustering using 7 acoustic classes. The grid is**
439   **resampled to a size of 100 m by 100 m. The black square indicates the extent of the area zoomed in Fig. 9 and Fig. 10.**

5. Discussion

441   In this section the repeatability of the classification results is discussed by comparing the

442   different surveys. The assignment of acoustic classes to sediment classes based on the

443   correlation of ground truth data with acoustic classes is also examined. Furthermore, the

444   spatial resolution and the reliability of the classification results is analysed. Finally, the

445   relationship between median grain size and backscatter values is investigated.

5.1   Repeatability and consistency of classification results

447   In order to examine the repeatability of the classification results over the different surveys, a

448   small area of the Cleaver Bank is shown in Fig. 9 and Fig. 10 with a total of ten intersections

449   of survey lines. All five surveys are represented in this small area of the map. Clearly there is

450   a high agreement in the classification results obtained from the data from different surveys.

451   Examples are the intersection of the easternmost 2013 week 45 vertical line that intersects

452   with the 2015 diagonal line (indicated by area D in the plot). In this intersection features as

453   narrow as eight meters are clearly visible and are in very good agreement for the two surveys.

454   At the intersection of the most western 2013 week 45 line and the 2013 week 47 line (area A)

455   both surveys show an area of acoustic class 3, surrounded by class 6. Area B indicates for

456   both surveys the presence of acoustic classes 2 to 6 in good agreement. The high repeatability

457   is also apparent in Fig. 11. Here the Bayes acoustic classes determined for the intersecting

458   areas of the 2013 and 2014/2015 surveys are presented in a scatter plot. It is shown that for

459   the majority of the cases the results are in good agreement. However, discrepancies also

460   occur, for example at the intersection of the 2015 survey and the 2013 week 47 survey in area

461   C of Fig. 9 and 10 the 2013 data shows acoustic class 2 whereas the 2015 data shows acoustic

462   class 1 for PCA. The Bayesian results in this intersection show class 3 for the 2013 data and

463   class 2 for the 2015 data. This is the most apparent disagreement seen on this part of the map,

464 and there are a few plausible explanations for this and other disagreements. Firstly, even

465 though it would not be expected, it is possible that there was a sediment change from 2013 to

466 2015, that would explain why the discrepancy is present for both classification methods in

467 area C. To prove a sediment change at any point a grab sample from both periods at the

468 location would be required but this is not available. According to Fig. 11 there are

469 discrepancies between the 2013 and the 2014/2015 data but they are not greater than 1

470 acoustic class except for 1 instance. It is possible that the backscatter from locations with

471 different classifications are close to a class boundary and happen to fall within the 1 class

472 discrepancy range. A further reason for a mismatch could be a directional small-scale

473 morphological influence because of different sailing directions [46]. Given that this is data

474 from five different surveys carried out over the time period from 2013 to 2015 and that the

475 data were acquired by different vessels, crews, MBES systems and environmental conditions,
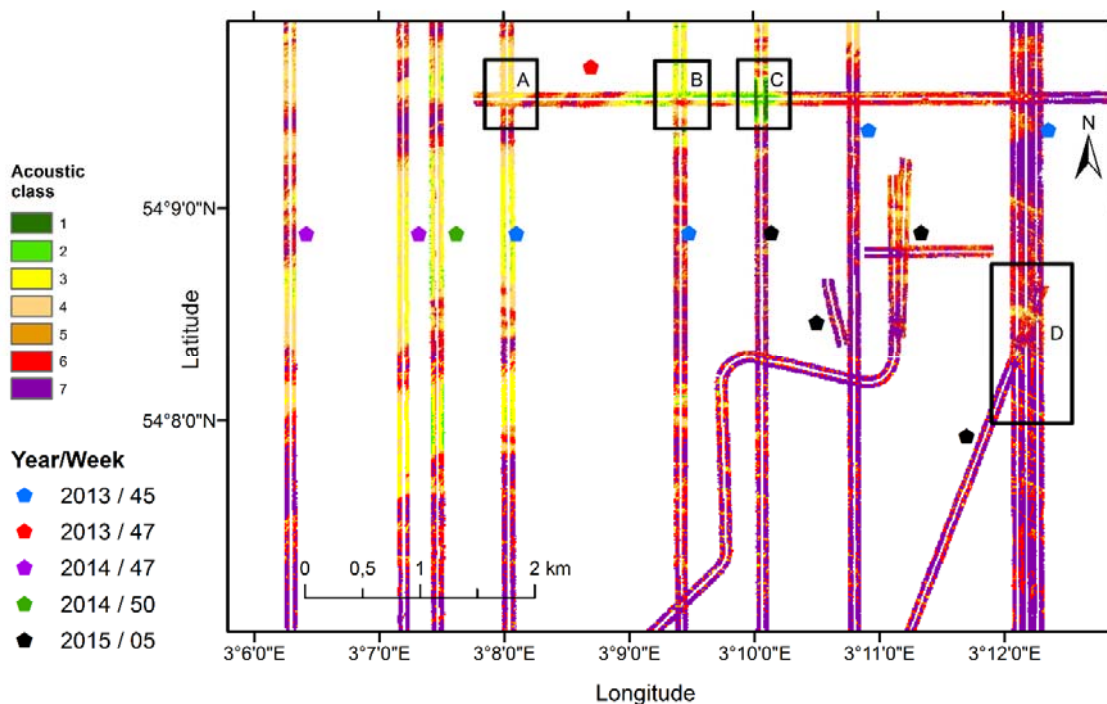

476

477 Fig. 9. Zoomed in area of acoustic class map generated by PCA. Different survey lines denoted by the coloured
478 pentagons are visible. The grid size is 10 by 10 m and represents the size of the surface patches.
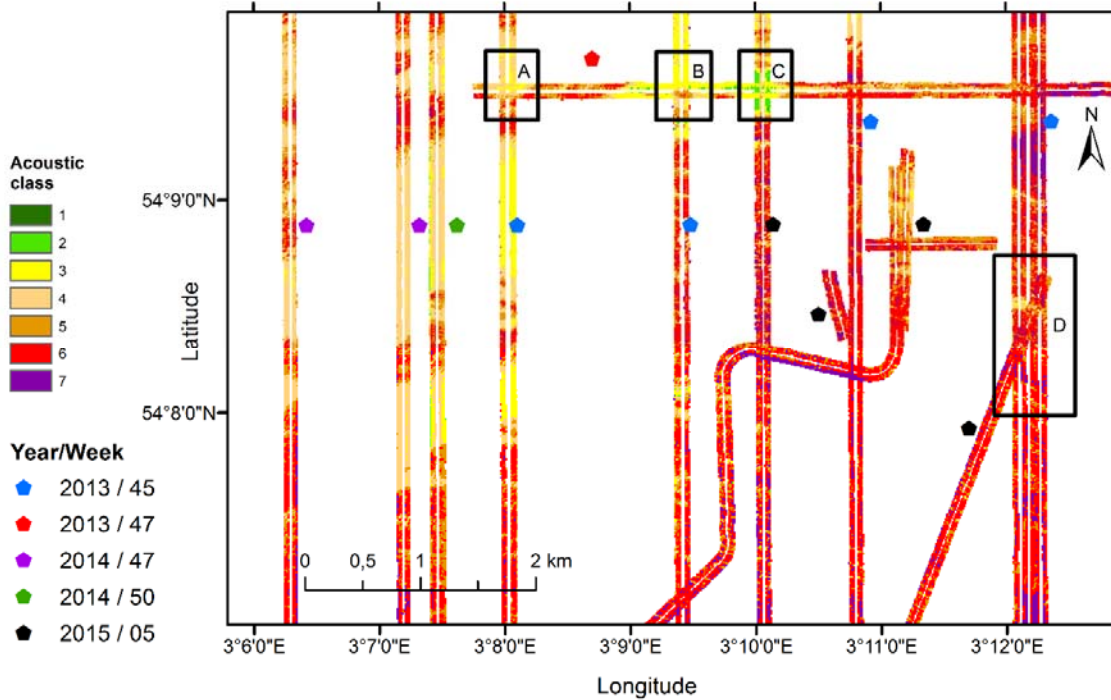
479

480 **Fig. 10. Zoomed in area of acoustic class map generated by Bayesian technique. Different survey lines denoted by the**
481 **coloured pentagons are visible. The grid is resampled to a size of 10 m by 10 m using the mode value of the finer grid.**
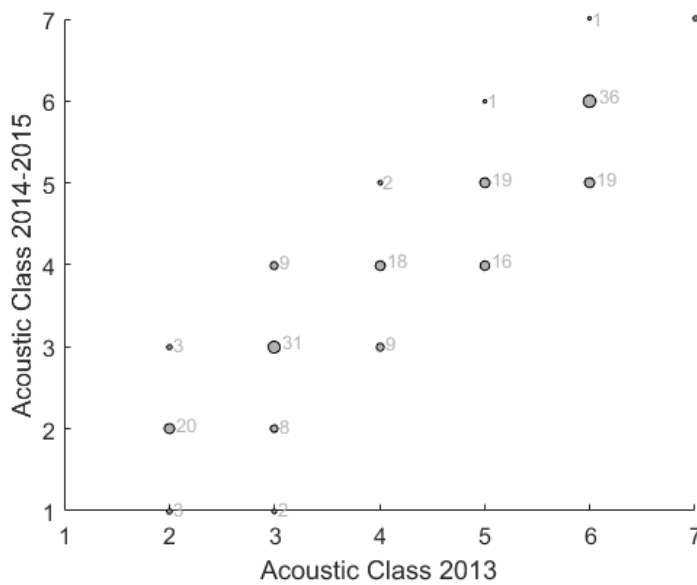
482

483 **Fig. 11. Correlation plot of the acoustic classes determined with the Bayesian method. The size of the dots and the**
484 **number indicate the number of matches for the acoustic classes determined for the intersecting areas using the**
485 **backscatter data from the different surveys in 2013, 2014, 2015.**

486 the results still demonstrate the high degree of repeatability and consistency of the acoustic

487 classifications for both methods. Although the classification results are in good agreement

488 when comparing the classification from different surveys for one method, the comparison

489 between classification results from applying different methods reveals differences. Whereas

490 the Bayes classification indicates the presence of mainly five types of sediments, since

491 acoustic classes 1 and 7 are hardly present, the PCA classification shows all sediment types to

492 be almost equally present. The deviations from PCA and Bayesian within the low and high

493 acoustic class ranges are related to the different mathematical approaches of the methods.

494 Considering Fig. 3, it is seen that the PDFs of acoustic class 1 and 7 have only a very small

495 contribution to the histogram of backscatter measurements. For k-means clustering 7 sediment

496 types are assumed. K-means clustering defines the clusters on a simple similarity

497 measurement of the first PC and assigns these clusters based on an increasing backscatter

498 value. This leads to a more balanced number of data points within the individual clusters, i.e.,

499 acoustic classes. Therefore, the PCA results show, in contrast to Bayes, a significant presence

500 of acoustic class 1 and 7. Still, the maps obtained with the two different methods indicate a

501 similar spatial distribution of the different sediment types over the area.

502 **5.2 Mapping Folk class by combining acoustic classes with ground truth data**

503 Often, for mapping the spatial distribution of sediments, use is made of maps presenting the

504 Folk class. Here it is investigated to what extent these types of maps can be derived from the

505 acoustic classification results by assigning sediment types to the acoustic classes. For this, we

506 use the grab samples that are located at a distance less than 25 m from a survey track, i.e.

507 slightly more than the 20 m recommended in [46], and that are in areas with little spatial

508 variation in sediment type. As such, the initial 104 grab samples (Fig. 1) are reduced to 77

509 grab samples.

510 As a first step, it is assumed that the lowest acoustic class represents finer sediments whereas

511 the highest acoustic class represents coarser sediments. Here the order of Folk classes is

512   selected such that it is assumed to represent increasing median grain size. The resulting

513   number of matches between acoustic class number and sediment type at the grab sample

514   location are plotted in Fig. 12 for the Bayes and PCA results, respectively. In general, indeed

515   increasing acoustic class is seen to correspond to an increasing median grain size, as

516   represented by the sediment type.

517   The PCA results show a good match of acoustic class 1 with the sediment type sandy mud.

518   For example, this indicates that the Botney cut is covered by sandy mud. However, the

519   assignment of the sand sediment types from muddy sand to sandy gravel are less clear. For

520   instance, the sediment type sand shows a uniform distribution from acoustic class 1 to 5. This

521   indicates additional factors influencing the backscatter data and causes difficulties in the

522   assignment of sediment type sand to a distinct acoustic class. For the Bayes results (Fig. 12a) it

523   is found that acoustic class 1 does not correlate to any grab sample. For all other acoustic

524   classes there is some ambiguity in the relation between sediment type and acoustic class.

525
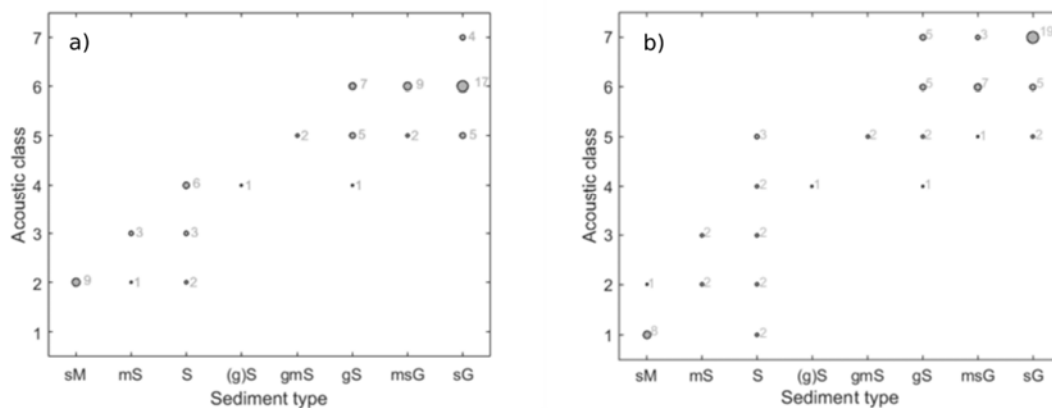
Fig. 12. Correlation between acoustic class and sediment type at grab sample locations. a) Bayesian method, b) PCA.
Dots indicate the number of matches between acoustic class and sediment type. The sediment type is determined after
Folk [22].

529   Fig. 13 shows the Folk class map based on the Bayes classification accounting for the

530   mentioned non-uniqueness. The proposed assignment of Folk class to sediment type used is

531   presented in table 2. It should be noted, however, that especially for acoustic class 5 a unique

532   relation with Folk class is not found and for Fig. 13 it is taken to correspond mainly to

533 gravelly sand and muddy sandy gravel. A similar map can be made for the results of PCA, but

534 here only the Bayes results in Fig. 13 are presented.

535 **Table 2 Assignment of sediment type (Folk scheme) to acoustic class. Acoustic classes are obtained from applying the**
536 **Bayes classification method.**

Sediment type	**sM** sandy mud	**mS** muddy sand	**S** sand	**gmS** gravelly muddy sand	**gS** gravelly sand	**msG** muddy sandy gravel	**sG** sandy gravel
Acoustic class	2	3	4	5	5-6	5-6	6-7

537

5.3 Spatial resolution of classification results

539 To investigate the scale of information obtained from the acoustic classification, Fig. 13

540 shows more detailed pictures of selected areas in the Cleaver Bank. These areas are selected

541 because grab samples are available and abrupt changes in the acoustic class occur within a

542 mainly homogeneous area. Whereas, on the main sediment map the high resolution and the

543 agreement between grabs sample and classification result are not obvious, the zoomed in plots

544 do demonstrate these items. Each picture depicts strong changes in sediment classes over tens

545 of meters resolved by the acoustic classification method. The sediment type of the grab

546 samples denoted by the coloured squares matches well with the classification result. In

547 particular, Fig. 13b shows an abrupt change in the sediment map which matches perfectly

548 with the ground truth given sandy gravel and sand as a sediment type. It is notable that the

549 sand grab sample is only approximately 10 m away from the estimated sand to gravel

550 boundary but is perfectly resolved on the sediment map. Fig. 13c displays an area which

551 seems to be a homogeneous sandy mud to muddy sand region on the main map but the

552 detailed view reveals a gravelly sediment patch within this area. This patch matches very well

553 with the grab sample of muddy sandy gravel. The detailed pictures display only a few

554 examples of the match between classification result and grab sample. The main map of the

555 Cleaver Bank, in general, also shows good agreement between classification results and

556   ground truth. For instance, the Botney cut is classified with sandy mud which fits to each grab

557   sample taken in that area.
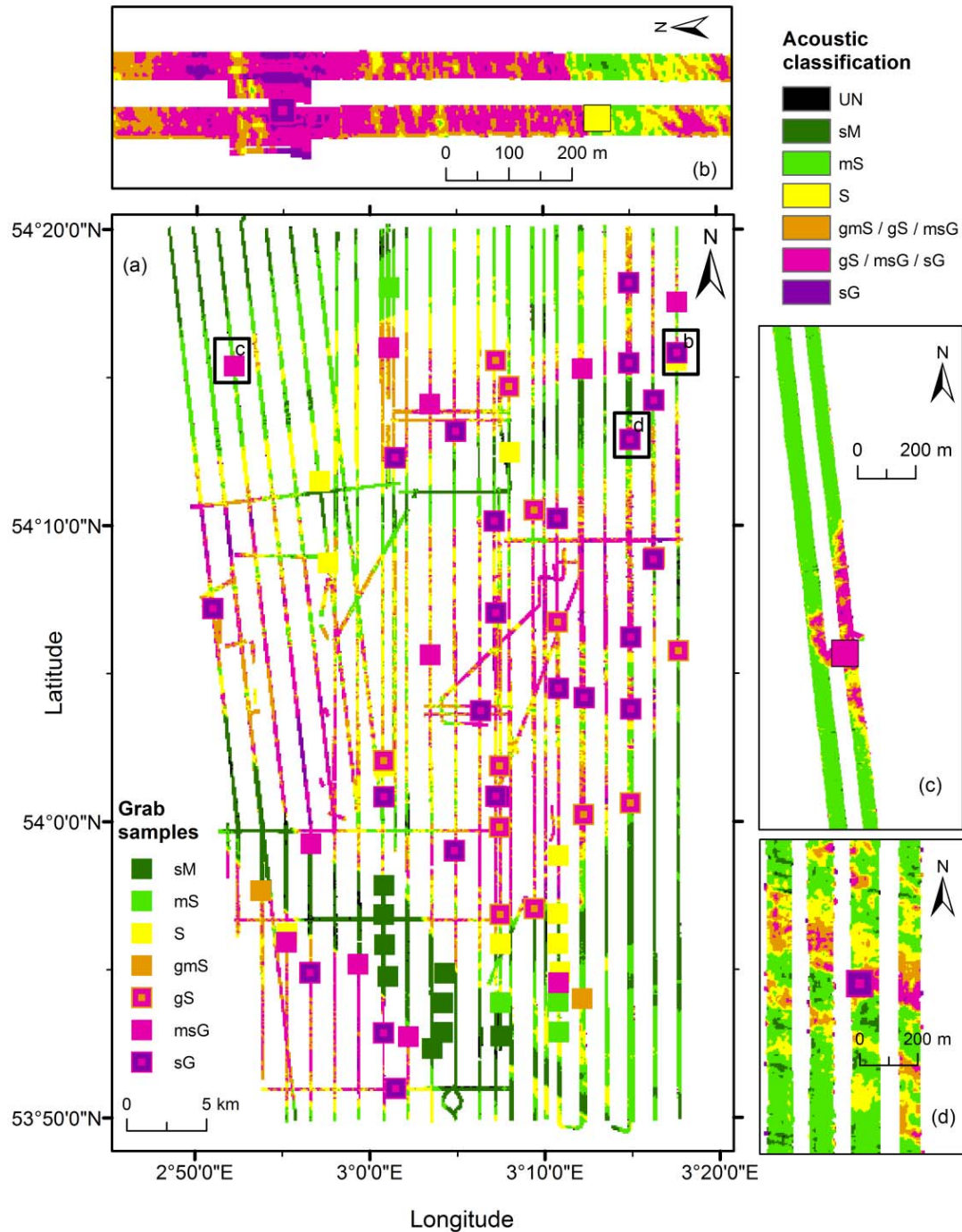
558

559   **Fig. 13. Sediment map of the Cleaver Bank obtained from the Bayesian method and ground truth data. Sediment**
560   **classes range from sandy mud (sM) to sandy gravel (sG). a) Sediment map of the entire survey area of the Cleaver**
561   **Bank with a resolution of 100 m by 100 m. b), c) and d) represent small areas of the sediment map with a resolution of**
562   **3 m by 3 m. The grab samples can be seen in the main map as a colour coded squares.**

563 **5.4   Relation of acoustic classes with sediment median grain size**

564 In Section 5.2 the relation between acoustic class and Folk class is investigated. It is found

565 that no unique relation holds for the frequency and sediments considered in this study.

566 Therefore, in this section it is investigated whether a more unique relationship between

567 acoustic class and median grain size exists. To this end, the median grain sizes (D50 value) of

568 the grab samples are now considered as in [47]. Except for class 7, the median values increase

569 with class number as seen in Fig. 14 which presents the median of the D50 values as a

570 function of acoustic class. This reflects an increasing backscatter value with increasing class

571 number. Class 7 does not have a mean or median value higher than that of class 6. This

572 indicates a situation where the highest backscatter values (class 7) apparently correspond to

573 median grain sizes that are not necessarily higher than those belonging to class 6. Based on

574 this result it can be concluded that, especially for the higher acoustic classes, as for the Folk

575 class also no unique relationship between acoustic class and median grain size exists in the

576 data.

577 To further investigate this we consider standardized backscatter values instead of acoustic

578 class. In Fig. 15 the backscatter values (averaged over measurements within 25 m around a

579 grab sample location) are shown as a function of D50 values. The backscatter values are

580 additionally normalized by dividing each backscatter value by the maximum backscatter value

581 thus yielding values strictly between -1 and 1. Fig. 15 shows a significant positive correlation

582 between backscatter and median grain size for the fine fraction ($< 1\phi$ (0.5 mm)). From the

583 data, however, it is found that the magnitude of increase in backscatter with increasing median

584 grain size is less significant between 1 and -1 ϕ (0.5 mm - 2 mm), followed by a plateau and a

585 decrease for even coarser sediments. This indicates an ambiguity for the relationship between

586 backscatter values and median grain size exists and hinders the discrimination of sediment

587 types with median grain sizes larger than 1 ϕ (0.5 mm) using acoustic classification methods

588   based only on backscatter data. This is in agreement with the findings of section 5.2. and

589   indicates that there is no one-to-one relationship between median grain size and backscatter

590   for the entire grain size spectrum. Such a positive correlation between backscatter and median

591   grain size followed by a negative correlation was also observed in [4]. They referred to this

592   change in relationship as a transition point. The transition point in the study of [4] occurred at

593   -3.5 ϕ (11 mm) using a frequency of 300 kHz. We estimate the transition point at

594   approximately -2 ϕ (4 mm). The transition point in [4] and the transition point in this study

595   both occur roughly around the acoustic wavelength (5 mm) of the MBES.
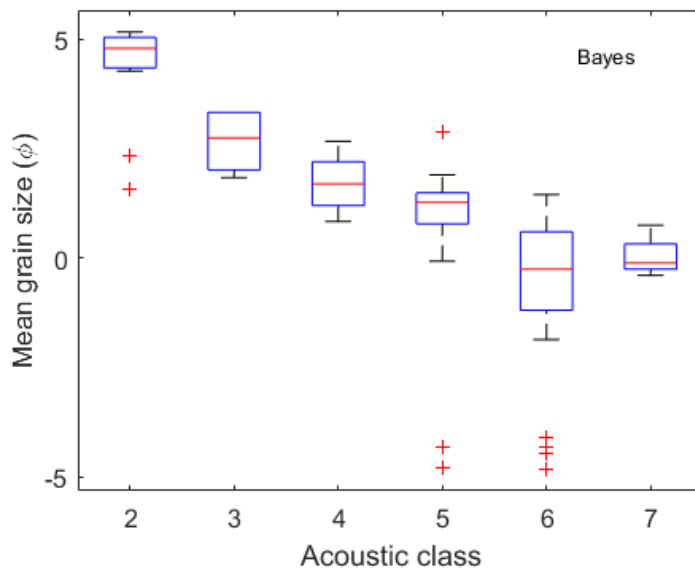
596

597   **Fig. 14. Box plots of sediment samples that fall within the same acoustic class. The bottom and top of the blue**
598   **rectangle represent the 25th and 75th percentiles, respectively, whereas the red line indicates the median value. The**
599   **whiskers extend to the minimum and maximum value of the D50 values that are not considered outliers (i.e. they are**
600   **no more than ±2.7σ apart). Outliers are marked with red crosses. The results for PCA, not plotted, are very similar.**
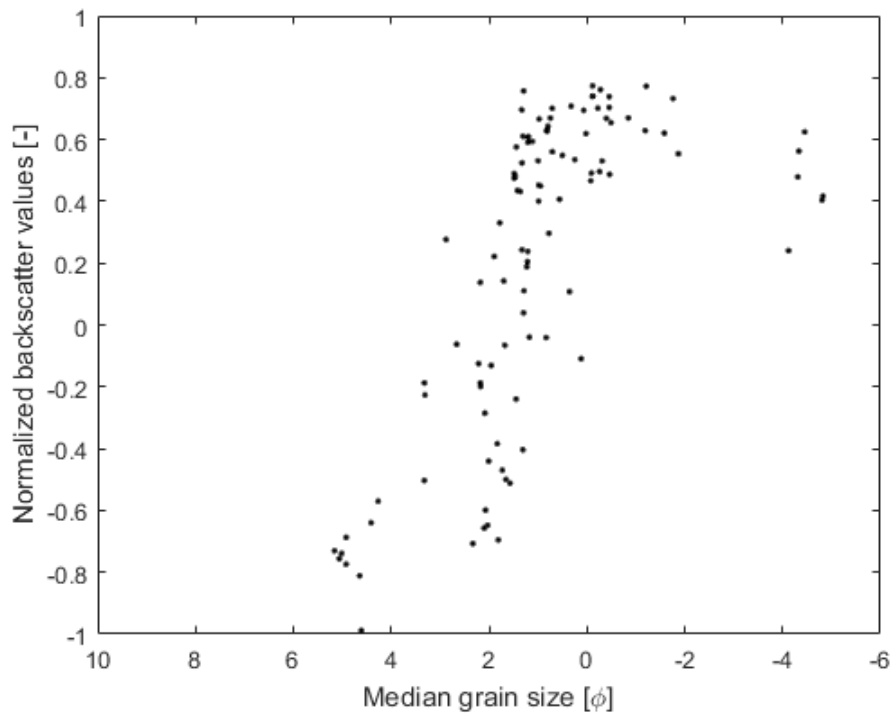
601

602

603 **Fig. 15. Backscatter values as a function of the median grain size (D50) of grab samples. Dots indicate the averaged**
604 **and standardized backscatter values within a maximum radius of 25 m around the grab sample.**

605

6. Summary and conclusions

607 In this study two different acoustic classification methods, namely the Bayesian method and

608 the PCA in conjunction with k-means clustering, were applied to MBES backscatter data from

609 the Cleaver Bank in the Dutch North Sea. For both methods, the classification is based on

610 changes in backscatter values for different sediment types. The data were acquired on two

611 different Dutch vessels during five different surveys carried out in various time periods from

612 2013 to 2015.

613 The resulting maps show a high consistency between the classification results obtained from

614 the different surveys and using a single classification method, despite the use of different

615 vessels and varying time periods. Some discrepancies are observed (a difference of 1 acoustic

616 class); to gain a better understanding of these would require repeated surveys following the

617 same survey patterns and supported by repeated grab samples for each of those surveys.

618 Despite the discrepancies, this study demonstrates the potential of using backscatter data for

619 achieving repeatable seabed sediment classification results even if the backscatter data is

620 acquired during different time periods and from MBES systems which are mounted on

621 different ships and thus subjected to different calibrations, survey settings, and ship crews. It

622 can be concluded that the current state of MBES sediment classification techniques is such

623 that it can be applied for marine sediment monitoring purposes where the aim is to identify

624 changes in the sediment over time.

625 However, the current study clearly shows that monitoring requires the use of a single

626 classification technique. Although, the same large-scale features are resolved, the two

627 different techniques result in different maps. For the two techniques considered and using

628 backscatter data only, the difference fully stems from the different approaches used for

629 assigning backscatter measurements to a certain acoustic class. The Bayesian technique

630 accounts for the statistical characteristics of the backscatter by assuming Gaussian distributed

631 backscatter values. Whereas PCA in conjunction with the k-means algorithm uses a cluster

632 technique to classify a dataset with respect to similarities of predefined properties and,

633 thereby, neglects the natural fluctuation of backscatter which can superimpose the backscatter

634 variation due to different seabed properties. The latter was found to underestimate the number

635 of sediment types within the study area. Still, if additional information, such as bathymetry

636 derived features, is considered the PCA method becomes an essential tool due to the ability of

637 selecting the most valuable features [4], [20].

638 Finally, it was investigated to what extent Folk classes and median grain sizes can be assigned

639 to acoustic classes. In general, this step is hindered by the fact that sediment bulk density,

640 seafloor roughness, volume heterogeneity, discrete scatterers and sediment layering all

641 contribute to backscatter strength depending on the seabed complexity, acoustic frequency

642 and incident angle [1], [2], [3]. For the Cleaver Bank area and the multi-beam (300 kHz)

643 considered here, no unique relation between Folk class and acoustic class could be

644 established. To still be able to map Folk class, a conversion scheme accounting for this non-

645 uniqueness was introduced where a range of Folk classes is assigned to a single acoustic class.

646 With regards to the relationship between median grain size and backscatter (acoustic class), a

647 strong positive correlation for the fine fraction (< 0.5 mm) followed by a decrease in positive

648 correlation and a change into negative correlation for coarser sediments (> 4 mm) are

649 observed. This constitutes an ambiguity in the relationship between backscatter and median

650 grain size. Therefore, care must be taken when assigning sediment properties or types (e.g.

651 median grain size or Folk class) to an acoustic class based on MBES backscatter.

652 In conclusion, although limitations exist, current seafloor classification capabilities are such

653 that they are a valuable asset in long-term monitoring efforts of the marine environment.

7. Acknowledgements

659

660

661 **Bibliography**

662

[1] D. R. Jackson and M. D. Richardson, High-Frequency Seafloor Acoustics, New York: Springer Science, 2007.

[2] A. N. Ivakin, "Scattering from discrete inclusions in marine sediments," in *Proc. Seventh European Conference on Underwater Acoustics. Delft University of Technology*, Delft, The Netherlands, 2004.

[3] K. L. Williams, D. R. Jackson, D. Tang, K. B. Briggs and E. I. Thorsos, "Acoustic backscattering from a sand and a sand/mud environment: Experiments and data/model comparison," *IEEE Journal of Oceanic engineering,* vol. 34, no. 4, pp. 388-398, 2009.

[4] D. Eleftherakis, M. Snellen, A. Amiri-Simkoeei and D. G. Simons, "Observations regarding coarse sediment classification based on multi-beam echo-sounder's backscatter strength and depth residuals in Dutch rivers," *J. Acoustic. Soc. Am.,* vol. 135, no. 6, pp. 3305-3315, 2014.

[5] J. S. Collier and C. J. Brown, "Correlation of sidescan backscatter with grain size distribution of surficial seabed sediments," *Marine Geology,* vol. 214, no. 4, pp. 431-449, 2005.

[6] G. De Falco, R. Tonielli, G. Di Martino, S. Innangi, S. Simeone and I. M. Parnum, "Relationships between multibeam backscatter, sediment grain size and Posidonia oceanica seagrass distribution," *Continental Shelf Research,* vol. 30, pp. 1941-1950, 2010.

[7] J. A. Goff, H. C. Olson and C. S. Duncan, "Correlation of side scan backscatter intensity with grain size distribution of shelf sediments," *Geo-marine Letters,* vol. 20, pp. 43-49, 2000.

[8] T. Medialdea, l. Somoza, R. F. M. Leon, G. Ercilla, A. Maestro, D. Casas, E. Llave, F. J. F.-P. M. C. Hernandez-Molina and B. Alonso, "Multibeam backscatter as a tool for sea-floor characerization and identification of oil spills in the Galicia Bank," *Marine Geology,* vol. 249, pp. 93-107, 2008.

[9] D. G. Simons, M. Snellen and M. Ainslie, "A multivariate correlation analysis of high-frequency bottom backscattering strength measurements with geotechnical parameters," *IEEE J. Ocean. Eng.,* vol. 32, pp. 640-650, 2007.

[10] B. D. Edwards, P. Dartnell and H. Chezar, "Characterizing benthic substrates of Santa Monica Bay with seafloor photography and multibeam sonar imagery," *Marine Environmental Research,* vol. 56, no. 1-2, pp. 47-66, 2003.

[11] V. E. Kostylev, R. C. Courtney, G. Robert and B. J. Todd, "Stock evaluation of giant scallop (Placopeceton magellanicus) using high-resolution acoustics for seabed mapping," *Fisheries Research,* vol. 60, no. 2-3, pp. 479-492, 2003.

[12] J. C. Borgeld, J. E. Hughes Clark, J. A. Goff, L. A. Mayer and J. A. Curtis, "Acoustic backscatter of he 1995 flood deposit on the Eel shelf," *Marine Geology,* vol. 154, pp. 197-210, 1999.

[13] F. O. Nitsche, R. Bell, S. M. Carbotte, W. B. F. Ryan and R. Flood, "Process-related classification of acoustic data from the Hudson River Estuary," *Marine Geology,* vol. 209, pp. 131-145, 2004.

[14] L. Fonseca, L. Mayer, D. Orange and N. Driscoll, "The high-frequency backscattering angular response of gassy sediments: model/data comparison from Eel River Margin, California," *The Journal of the Acoustical Society of America,* vol. 111, no. 6, pp. 2621-2631, 2002.

[15] K. Siemes, M. Snellen, A. R. Amiri-Simkooei, D. G. Simons and J.-P. Hermand, "Predicting Spatial Variability of Sediment Properties From Hydrographic Data for Geoacoustic Inversion," *IEEE Journal of Oceanic Engineering,* vol. 35, no. 4, pp. 766-778, 2010.

[16] C. McGonigle and J. Collier, "Interlinking backscatter, grain size and benthic community structure," *Estuar. Coast. Shelf Sci.,* vol. 147, pp. 123-136, 2014.

[17] D. D. Sternlicht and C. P. de Moustier, "Remote sensing of sediment charactristics by opitmized echo-envelope matching," *The Journal of the Acoustical Society of America,* vol. 114, no. 5, pp. 2727-2743, 2003.

[18] L. Fonseca, C. Brown, B. Calder, L. Mayer and Y. Rzhanov, "Angular range analysis of acoustic themes from Stanton banks Ireland: a link between visual interpretation and multibeam echosounder angular signatures," *Applied Accoustic,* vol. 70, pp. 1298-1304, 2009.

[19] C. J. Brown, B. J. Todd, V. E. Kostylev and R. A. Pickrill, "Image-based classification of multibeam sonar backscatter data for objective surficial sediment mapping of Georges Bank, Canada," *Continental Shelf Research,* vol. 31, pp. 110-119, 2010.

[20] D. Eleftherakis, A. Amiri-Simkooei, M. Snellen and D. G. Simons, "Improving riverbed sediment classification using backscatter and depth residual features of mulit-beam echo-sounder systems," *J. Acoust. Soc.,* vol. 131, no. 5, pp. 3710-3725, 2012.

[21] J. Anderson, D. van Holliday, R. Kloser, D. Reid and Y. Simard, "Acoustic seabed classification: current practice and future directions," *ICES Journal of Marine Science,* vol. 65, pp. 1004-1011, 2008.

[22] C. J. Brown, S. J. Smith, P. Lawton and J. T. Anderson, "Benthic habitat mapping: A review of progress towards improved understanding of the spatial ecology of the seafloor using acoustic techniques," *Estuarine, Coastel and Shelf Science,* vol. 92, pp. 502-520, 2011.

[23] D. G. Simons and M. Snellen, "A Bayseian approach to seafloor classification using multi-beam echo-sounder backscatter data," *Applied Acoustics,* vol. 70, pp. 1258-1268, 2009.

[24] E. Alevizos, M. Snellen, D. G. Simons, K. Siemens and J. Greinert, "Acoustic discrimination of relatively homogeneous fine sediments using Bayesian classification on MBES data," *Marine Geology,* vol. 370, pp. 31-42, 2015.

[25] E. Heffron, M. Doucet, C. Brown, G. Lamarche and R. Cooper, "Multibeam Backscatter Workshop - State of the Technology, Tools & Techniques: Overview," GeoHab Annual Conference,

Fiorentino, A., Rome, Italy, 2013.

[26] X. Lurton, G. Lamarche, C. Brown, V. Lucieer, G. Rice, A. Schimel and T. Weber, "Backscatter measurements by seafloor-mapping sonars. Guidelines and Recommendations," 2015.

[27] H. J. Lindeboom, R. Witbaard, O. G. Bos and E. Meesters, "Gebiedsbescherming Noordzee. Habitattypen, instandhoudingsdoelen en beheersmaatregelen," *Wettelijke Onderzoekstaken Natuur & Milieu,* vol. 114, 2008.

[28] N. Schrieken, A. Gittenberger, J. W. P. Coolen and W. Lengkeek, "Marine fauna of hard substrata of the Cleaver Bank and Dogger Bank," *Nederlandse Faunistische Mededelingen,* vol. 41, pp. 69-78, 2013.

[29] E. Hammerstedt, "EM technical note: backscattering and seabed image reflectivity 1-5," 2000.

[30] R. L. Folk, "The distinction between grain size and mineral composition in sedimentary-rock nomenclature," *J Geol,* vol. 62, no. 4, pp. 344-359, 1954.

[31] EMODnet, "http://www.emodnet-hydrography.eu/," European Marine Observation and Data Network, 2016. [Online]. [Accessed 5 August 2016].

[32] A. R. Amiri-Simkooei, M. Snellen and D. G. Simons, "Riverbed sediment classification using multi-beam echo-sounder backscatter data," *J. Acoust.,* vol. 126, pp. 1724-1738, 2009.

[33] K. Pearson, "On lines and planes of closet fit to systems of points in space," *Philos. Mag.,* vol. 2, no. 6, pp. 559-572, 1901.

[34] H. Hotelling, "Analysis of a complex of statistical variables into principal components," *J. Educ. Psychol.,* vol. 24, no. 7, pp. 498-520, 1933.

[35] P. R. Bevington and D. K. Robinson, Data Reduction and Error Analysis for the Physical Sciences 3rd edition, New York: McGraw-Hill, 2003.

[36] Siswadi, A. Muslim and T. Bakhtiar, "Variable selection using principal component and procrustes analyses and ITS application in educational data," *Journal of Asian Scientific Research,* vol. 2, no. 12, pp. 856-865, 2012.

[37] M. J. Canty, Image Analysis, Classification and Change Detection in Remote Sensing with Algorithms for ENVI/IDL, Boca Raton: CRC Press, Taylor & Francis Group, 2007.

[38] R. Tibshirani, G. Walther and T. Hastie, "Estimating the number of clusters in a data set via the gab statistic," *J. R. Statist. Soc. B,* vol. 63, pp. 411-423, 2001.

[39] L. Kaufman and P. Rousseeuw, Findings Groups in Data: an Introduction to Cluster Analysis, New York: Wiley, 1990.

[40] D. Davies and D. Bouldin, "A cluster seperation measure," *IEEE Transactions on Pattern Analysis and Machine Intelligence,* Vols. PAMI-1, no. 2, pp. 224-227, 1979.

[41] X. Lurton, An Introduction to Underwater Acoustics, Heidelberg: Springer-Verlag, 2010.

[42] J. M. Preston, A. C. Christney, S. F. Bloomer and I. L. Beaudet, "Seabed Classification of Multibeam Sonar Images," in *MTS/IEEE Oceans 2001 Conference*, Honolulu, HI, 2001.

[43] A. N. Gavrilov and I. M. Parnum, "Fluctuations of Seafloor Bakscatter Data From Multibeam Sonar systems," *IEEE Journal of Oceanic Engineering,* vol. 35, no. 2, pp. 209-219, 2010.

[44] E. Jakeman and P. N. Pusey, "Significance of K distributions in scattering elements," *Physical Review Letters,* vol. 40, no. 9, pp. 546-550, 1978.

[45] L. Hellequin, J. M. Boucher and X. Lurton, "Processing of high-frequency multibeam echo sounder data for seafloor characerization," *IEEE Journal of Oceanic Engineering,* vol. 28, no. 1, pp. 78-89, 2003.

[46] T. F. Sutherland, J. Galloway, R. Loschiavo, C. D. Levings and R. Hare, "Calibration techniques and sampling resolution requirements for groundtruthing multi-beam acoustic backscatter (EM3000) and QTC VIEW classification technology," *Estuarine Coastel and Shelf Science,* vol. 75, pp. 447-458, 2007.

[47] E. Alevizos, T. Schoenning, K. Koeser, M. Snellen and J. Greinert, "Quantifying the fine-scale distribution of Mn-nodules: insights from AUV multi-beam and imagery data fusion," *Currently in press,* 2017.

663

664